Electronic Supplementary Material (ESI) for RSC Advances.

This journal is © The Royal Society of Chemistry

Improve the ORR/OER bifunctional catalytic performance with amorphous Mn oxides made by photochemical metal-organic deposition

Fan Bai, ‡[a] Yuxiu He, ‡[b] Lincheng Xu, [ac] Yue Wang, [a] Yan Wang, [a] Zhanzhong Hao, *[c] Fan Li *[a]

a. Faculty of Environment and Life sciences, Beijing University of Technology, Beijing, 100124, Beijing, P. R. China.
E-mail: vanadiumli@bjut.edu.cn
b. Beijing Office of Metrohm China Ltd, Beijing 100085, P. R. China.
c. College of Chemistry, Baotou Teachers College, Bao Tou 014030, P. R. China.
E-mail: 18438602389@163.com

Footnotes
* Corresponding authors
‡ These authors contributed equally to this work.

Synthesis of sample

In this work, we used photochemical metal-organic deposition (PMOD) method to synthesize amorphous manganese oxides.

We choose manganese (II) 2-ethylhexanoate (6% Mn, Alfa Aesar) as the organic manganese source. 7.1114 g manganese (II) 2-ethylhexanoate (1.25 mmol Manganese) is put in a watch glass. 5 mL N-hexane is added into the watch glass to cover the bottom. Then we add 0.3000 g carbon powder XC-72 (25 mmol Carbon) which works as the conductive agent into the watch glass. The whole watch glass is placed in a ultrasonic cleaner with ultrasonic frequency of 40 kHz and ultrasonic power of 50 W (KQ-50B, Kunshan Ultrasonic instruments Co., Ltd) for ultrasound-assisted dispersion 10 min to dispersed this mixture uniformly. Three watch glasses of mixture above are placed in a dark chamber with 254 nm and 185 nm UV 48 W light sources (BOT-III, Beijing Zhongyiboteng Tech Co.,Ltd) and co-irradiated for 24 h, 48 h and 72 h respectively. After UV irradiation, all three watch glasses were dried in drying oven at 60 °C for 2 h. The uniform film formed is the target amorphous manganese oxide material.

Amorphous manganese oxide MnO_x-PMOD with different UV treatments were named MnO_x-PMOD24, MnO_x-PMOD48 and MnO_x-PMOD72.

To composite amorphous manganese oxides with Ti_4O_7, 7.1114 g manganese (II) 2-ethylhexanoate (1.25 mmol Manganese) is put in a watch glass. 5 mL N-hexane is added into the watch glass to cover the bottom. We add 0.3000 g carbon powder XC-72 (25 mmol Carbon) which works as the conductive agent into the watch glass. After that, we add 0.3790 g Ti_4O_7 (1.25 mmol) into the mixture. Then the whole watch glass is placed in a ultrasonic cleaner with ultrasonic frequency of 40 kHz and ultrasonic power of 50 W (KQ-50B, Kunshan Ultrasonic instruments Co., Ltd) for ultrasound-assisted dispersion 10 min to dispersed this mixture uniformly. One watch glass of mixture above are placed in a dark chamber with 254 nm and 185 nm 48 W UV light sources (BOT-III, Beijing Zhongyiboteng Tech Co.,Ltd) and co-irradiated for 48 h. After UV irradiation, the watch glass is dried in drying oven at 60 °C for 2 h. Amorphous manganese oxide MnO_x composited with Ti_4O_7 was named MnO_x/Ti_4O_7-PMOD.

Electrochemical measurements

All of the electrochemical measurements were carried with a three-electrode system, including working electrode, reference electrode and rod counter electrode. The working electrode was chosen by different electrochemical measurements. For the cyclic voltammetry (CV), linear sweep voltammetry (LSV) and electrochemical impedance spectroscope (EIS) tests, a glassy carbon working electrode of diameter Φ = 5 mm controlled by the rotating disk electrode (RDE, IPS RRDE). As for chronoamperometry (CA) and polarization curves tests, a glassy carbon piece of 10*10 mm was used as working electrode. A Hg/HgO reference electrode (in 0.1 mol/L KOH, 0.165 V vs. RHE) was used as reference electrode and a carbon rod counter electrode (Φ = 2 mm) was used as counter electrode. A customized five-holes flask was used as electrolytic cell, filled with 0.1 mol/L KOH aqueous solution as electrolyte. The electrolyte was saturated in argon firstly in order to activate the system and then saturated in oxygen for further electrochemical measurements.

The CV and LSV tests were measured with saturated in oxygen 0.1 mol/L KOH aqueous solution at the scan rate of 10 mV/s. For LSV tests, the rotate speed of rotating disk electrode was chosen as 225, 400, 625, 900, 1225, 1600, 2025 and 2500 rpm. The curves of 1600 rpm were chosen for LSV images.

The EIS tests were measured with aerating oxygen continuously by aerator pipe at rotate speed of 1600 rpm.

The polarization curves tests were measured before and after 5000 cycles of CV tests for comparing ORR and OER catalytic stability of different catalytic material. Oxygen was essential during the whole measured process.

The CA tests were measured at potential of 0.68 V vs. RHE according to the potential of ORR. Oxygen was essential during the measured process.

The electrochemical active surface area (ECSA) for each system was estimated from the electrochemical double-layer capacitance (C_{DL}) of the catalytic surface and specific capacitance (C_S).[S1,S2] The formula was described as eq1:

$$ECSA = C_{DL}/C_S \quad \text{eq1}$$

As for C_S, it can be regarded as function of electrolyte system and adopted as 0.05 mF/cm^2.[S3,S4] To measure C_{DL}, a potential range in which non-Faradaic processes occur is determined from CV tests. The range is typically a 0.1 V potential window centered at the open-circuit potential (OCP) of the measured system. The formula was described as eq2:

$$i = \nu * C_{DL} \quad \text{eq2}$$

where i is double-layer current and ν is scan rate. Therefore, the CV tests were measured at range of ±0.06V vs. OCP in figure S9A-C. The scan rates were chosen as 20, 40, 60, 80 and 100 mV/s and i was current at the potential of OCP. A series of plots were described as i-ν curves with a slope equal to C_{DL} as shown in figure S9D.

The K-L equation can be calculated by eq3:

$$1/J = 1/J_L + 1/J_K = 1/(B\omega^{1/2}) + 1/J_K \quad \text{eq3}$$

where J is current density at a certain potential, J_L is dynamic current density, J_K limiting diffusion current density, ω is rotate speed and B is function of electron transfer numbers n. A series of plots were described as $(1/J)$-$(1/\omega^{1/2})$ curves with a slope equal to 1/B and then electron transfer numbers n can be calculated. The K-L equation of different catalytic material were shown in figure S11 and S12 at the rotate speed of 225, 400, 625, 900, 1225, 1600, 2025 and 2500 rpm and scan rate of 10 mV/s.

Preparation of carbon paper electrode (positive electrode in Li-O_2 battery)

The carbon paper electrode is prepared by spraying method in this study. With the mass ratio of 3:6:1, 0.03 g catalytic material, 0.06 g Super P conductive carbon black, 0.20 g 5% PVDF are put in a 50 mL beaker and 15 mL N-methylpyrrolidone is added in it. The mixture is under magnetic stirring for about 60 min to make it uniform. After the mixture slurry appears slightly viscous, it is transferred into the gas compressor spray gun. The beaker is cleaned with a total of 15 mL N-methylpyrrolidone for 3-5 times, and transferred the residue to the spray gun. A cleaned and dried 20 cm×20 cm carbon paper is fixed on a flat glass plate for spraying. The slurry is slowly and evenly sprayed on the surface of carbon paper until it is completely infiltrated. The carbon paper should be kept flat on the glass plate to prevent the slurry flowing on it. When the fluidity of the surface grout disappears, the second time spraying is carried out and the operation is repeated for several time until all the slurry is exhausted. The carbon paper covered with the active material is transferred into a vacuum drying oven for 24 h at 80℃. After that, it is cooled down to room temperature and stamped into circular sheets with 14 mm diameter by a slicer. The weight of active material is got through the weight difference between carbon paper circular sheet and blank carbon paper. The circular carbon paper electrodes are packed separately and kept in a vacuum drying oven for 24 h at 120℃. After cooling to room temperature, they are transferred to the glove box for battery assembling.

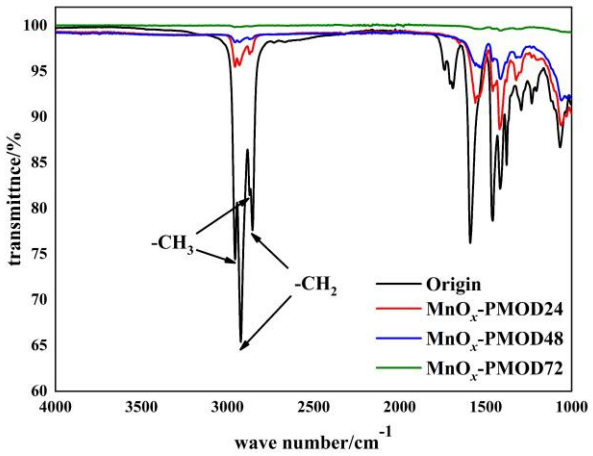

Figure S1 FTIR patterns of mixture before ultraviolet photolysis (Origin in Black) and amorphous manganese oxide MnO_x after ultraviolet photolysis of 24 h (MnO_x-PMOD24 in Red), 48 h (MnO_x-PMOD48 in Blue) and 72 h (MnO_x-PMOD72 in Green)

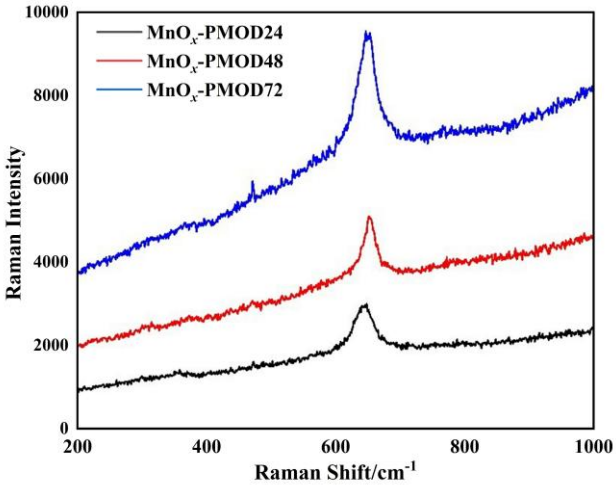

Figure S2 Raman patterns of amorphous catalysts MnO_x-PMOD24 (Black), MnO_x-PMOD48 (Red) and MnO_x-PMOD72(Blue)

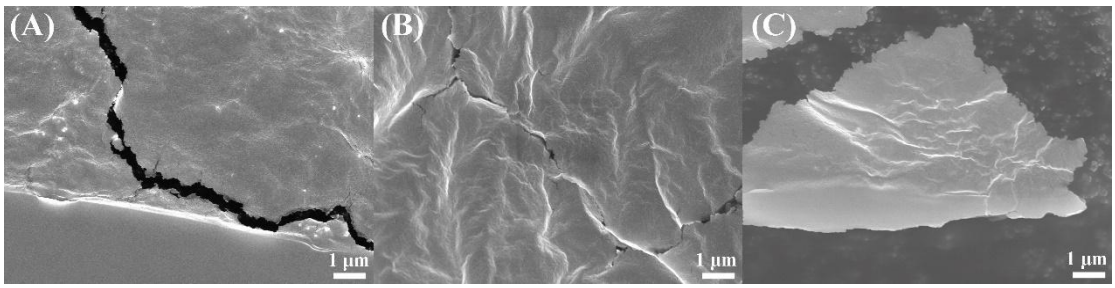

Figure S3 The SEM images show microstructure of amorphous catalysts (A) MnO_x-PMOD24，(B) MnO_x-PMOD48 and (C) MnO_x-PMOD72

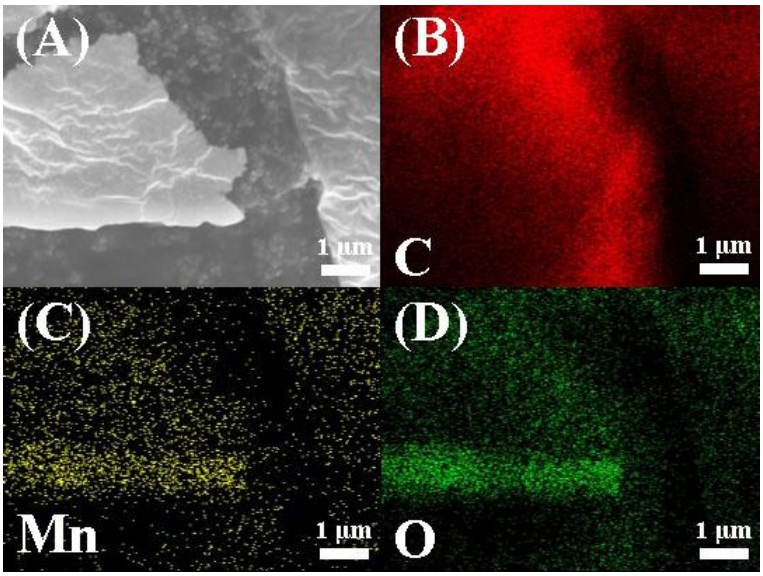

Figure S4 SEM and Energy dispersive spectrum (EDS) image of MnO_x-PMOD72

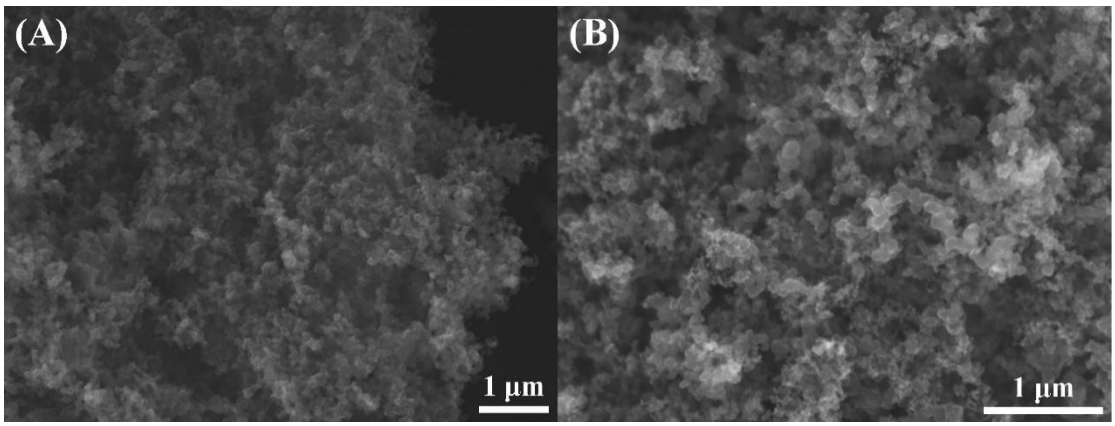

Figure S5 SEM images of (A) MnO_x-PMOD48 (B) XC-72 after ultrasonic dispersion

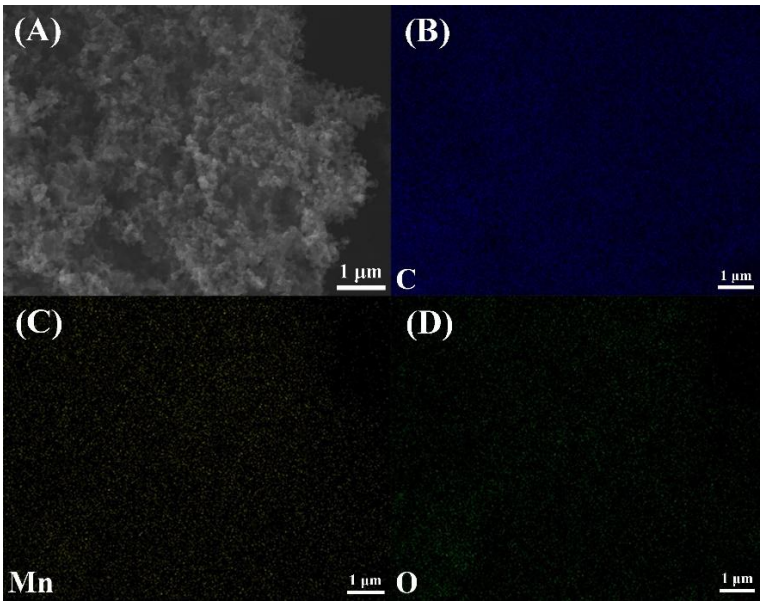

Figure S6 SEM and Energy dispersive spectrum (EDS) image of MnO_x-PMOD48 after ultrasonic dispersion

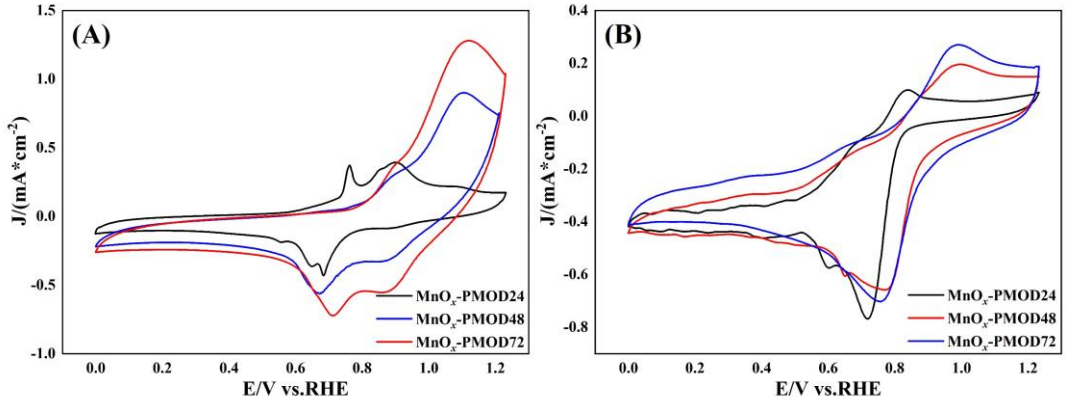

Figure S7 CV tests of MnO_x-PMOD24, MnO_x-PMOD48 and MnO_x-PMOD72, at the rate of 10 mV/s; saturated in (A) N_2 and (B) O_2

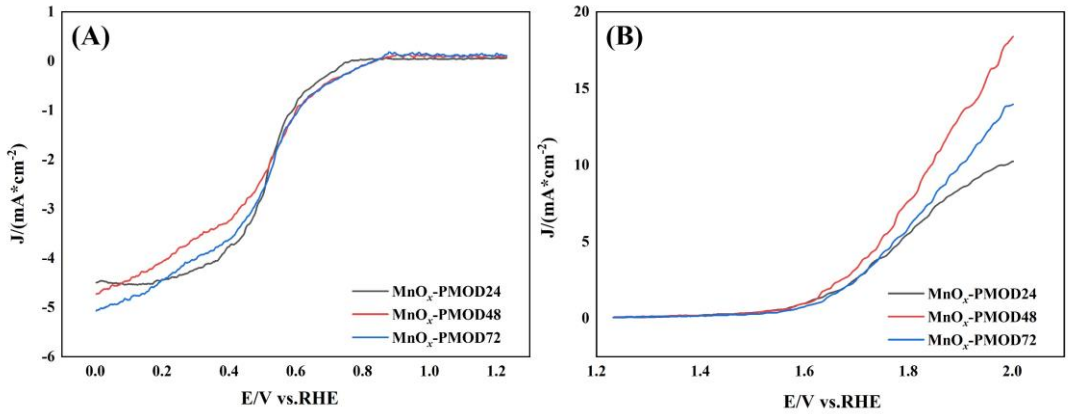

Figure S8 (A)ORR; (OER) curves of MnO_x-PMOD24, MnO_x-PMOD48 and MnO_x-PMOD72

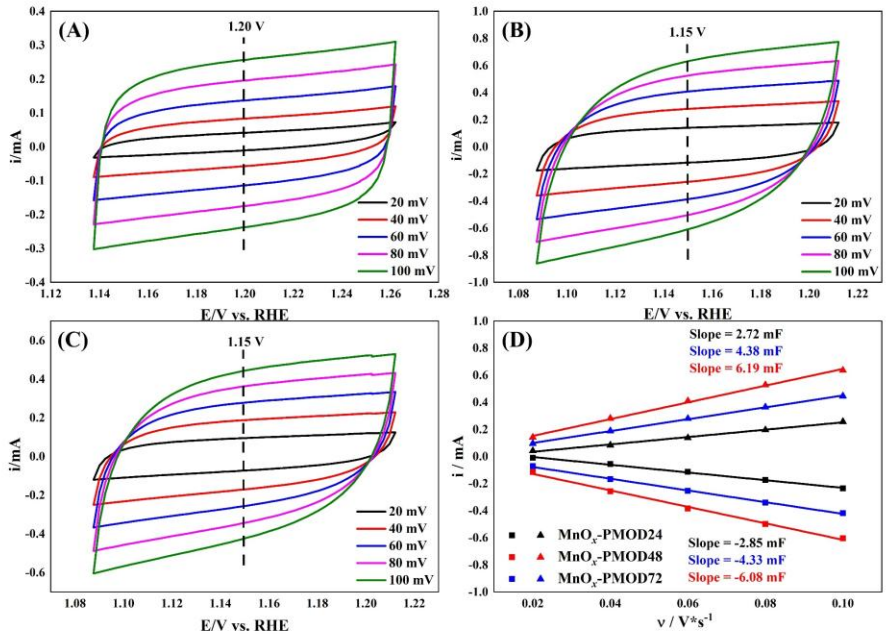

Figure S9 CV curves in a non-Faradaic region of (A) MnO_x-PMOD24, (B) MnO_x-

PMOD48 and (C) MnO_x-PMOD72，saturated in O_2；(D) The cathodic and anodic currents measured at OCP as a function of scan rates

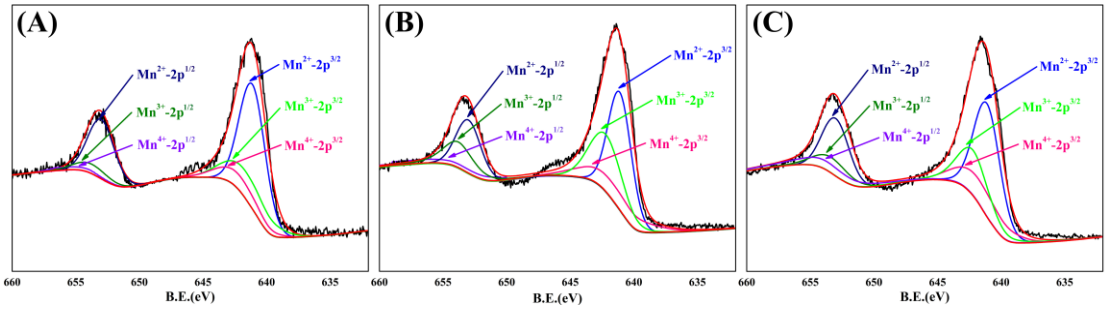

Figure S10. XPS patterns of Mn 2p of (A) MnO_x-PMOD24 (B) MnO_x-PMOD48 and (C) MnO_x-PMOD72

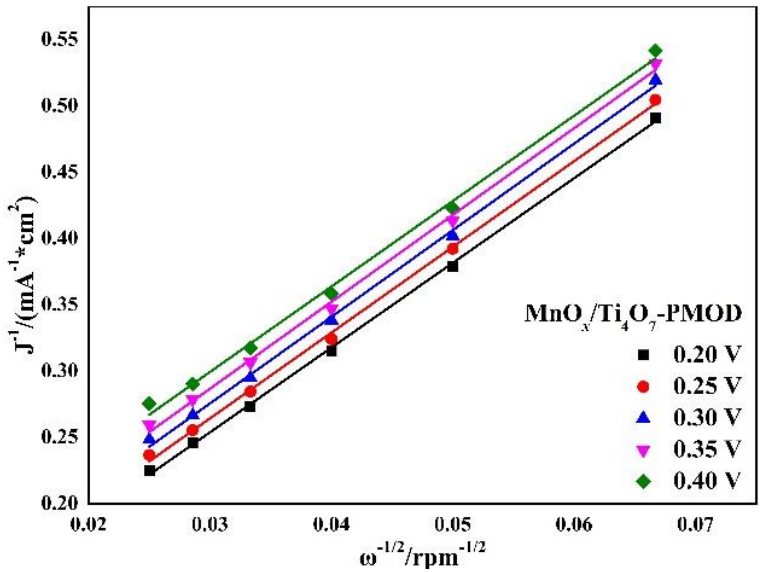

Figure S11. K-L equation fitting of amorphous catalyst MnO_x/Ti_4O_7-PMOD

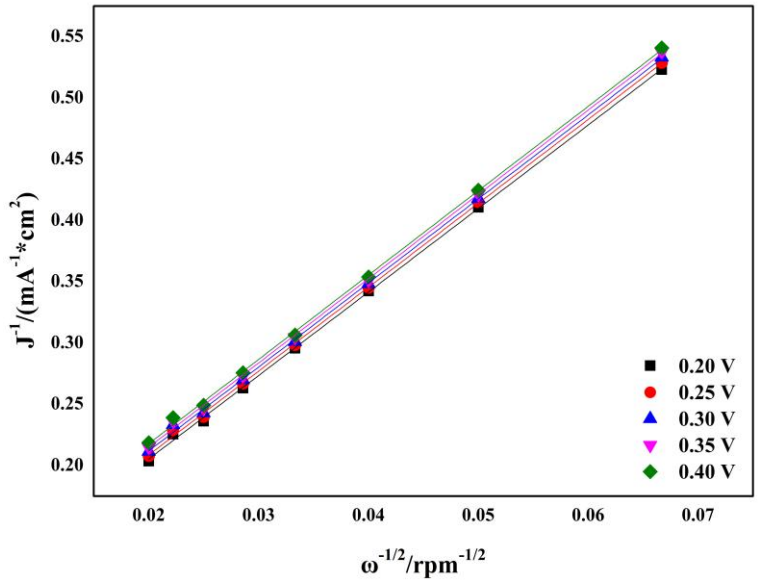

Figure S12. K-L equation fitting of crystalline catalyst MnO_x/Ti_4O_7-300

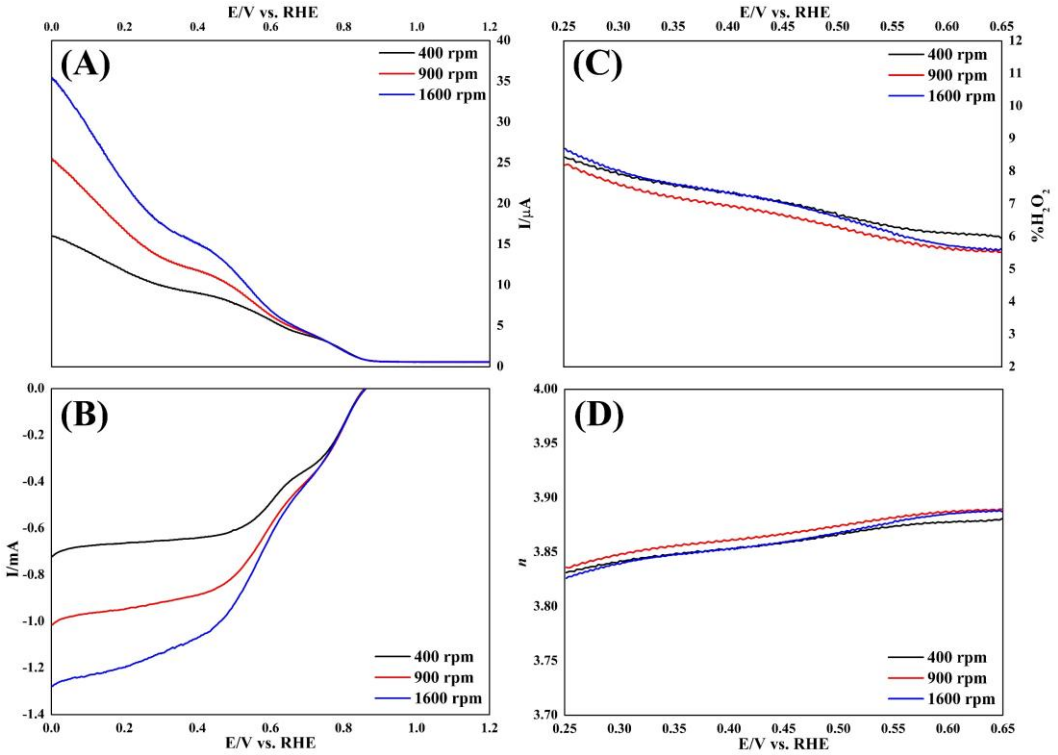

Figure S13. RRDE test of amorphous catalyst MnO_x/Ti_4O_7-PMOD. (A) ring current-potential, (B) disk current-potential, (C) $\%H_2O_2$ and (D) electron transfer numbers; saturated in O_2, at the rate of 10 mV/s

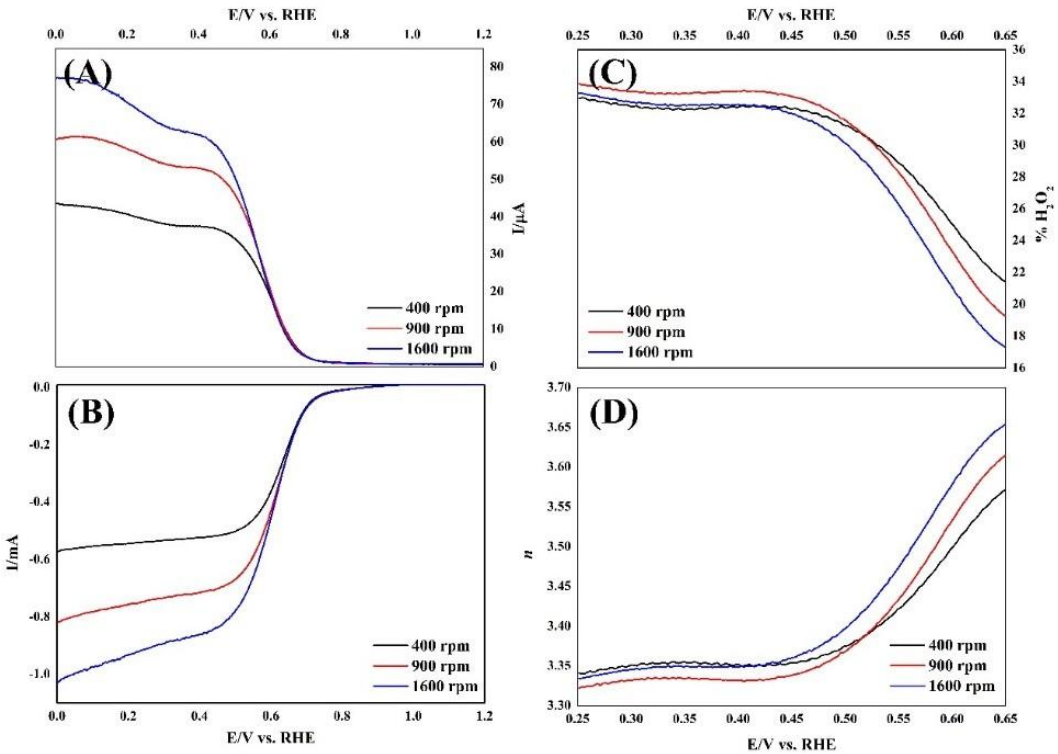

Figure S14. RRDE test of crystalline catalyst MnO_x/Ti_4O_7-300. (A) ring current-potential, (B) disk current-potential, (C) $\%H_2O_2$ and (D) electron transfer numbers; saturated in O_2, at the rate of 10 mV/s

Table S1 Valence state analysis of amorphous MnO_x samples after different ultraviolet light decomposition obtained from XPS

Sample name	orbit	Banding energy/eV	area	Ratio of $Mn^{2+}/Mn^{3+}/Mn^{4+}$
MnO_x-PMOD24	Mn^{2+}-$2p^{3/2}$	641.1	20758	0.693 0.221 0.086
	Mn^{2+}-$2p^{1/2}$	653.0	10379	
	Mn^{3+}-$2p^{3/2}$	641.6	6602	
	Mn^{3+}-$2p^{1/2}$	653.3	3301	
	Mn^{4+}-$2p^{3/2}$	642.2	2588	
	Mn^{4+}-$2p^{1/2}$	653.8	1294	
MnO_x-PMOD48	Mn^{2+}-$2p^{3/2}$	641.1	36884	0.539 0.291 0.170
	Mn^{2+}-$2p^{1/2}$	653.0	18442	
	Mn^{3+}-$2p^{3/2}$	641.6	19880	
	Mn^{3+}-$2p^{1/2}$	653.3	9940	
	Mn^{4+}-$2p^{3/2}$	642.2	11614	
	Mn^{4+}-$2p^{1/2}$	653.8	5807	
MnO_x-PMOD72	Mn^{2+}-$2p^{3/2}$	641.1	31838	0.483 0.278 0.239
	Mn^{2+}-$2p^{1/2}$	653.0	15919	
	Mn^{3+}-$2p^{3/2}$	641.6	18344	
	Mn^{3+}-$2p^{1/2}$	653.3	9172	
	Mn^{4+}-$2p^{3/2}$	642.2	15746	
	Mn^{4+}-$2p^{1/2}$	653.8	7873	

Table S2 Comparison of ORR/OER catalytic performance for benchmark noble metal and manganese oxide catalysts.

Catalysts	Electrolyte	Half-wave potential for ORR(V)	Overpotential for OER at 10 mA/cm^2(mV)	Ref.
Pt/C	0.1 M KOH	0.82	--	S5
PtGa NWs	0.1 M $HClO_4$	0.86	--	S6
IrO_2	1.0 M KOH	--	255	S7
RuO_2	0.1 M KOH	--	390	S8
NiFe-LDHs	1.0 M KOH	--	190	S9
α-MnO_2-SF	0.1 M KOH	0.78	490	S10
Mn_3O_4/Ti_3C_2	0.1 M KOH	0.85	--	S11
Mn_3O_4-NR	1.0 M NaOH	0.78	--	S12
Mn_3O_4	0.1 M KOH	--	Not achieve	S13
Our work	0.1 M KOH	0.72	Not achieve	S14
Our work	0.1 M KOH	0.75	530	This work

Table S3 Comparison of electrochemistry and battery performance for crystalline catalyst MnO_x/Ti_4O_7-300 and amorphous catalyst MnO_x/Ti_4O_7-PMOD

	MnO_x/Ti_4O_7-300	MnO_x/Ti_4O_7-PMOD
Onset potential for ORR	0.80 V vs. RHE	0.92 V vs. RHE
Half-wave potential for ORR	0.72 V vs. RHE	0.75 V vs. RHE
Limiting diffusion current for ORR	-4.34 mA/cm^2	-5.21 mA/cm^2
Onset potential for OER	1.71 V vs. RHE	1.60 V vs. RHE
Overpotential for OER at 10 mA/cm^2	Not achieve	530 mV
Number of electron transferred from K-L equation	3.87	3.89
Number of electron transferred from RRDE	3.40	3.87
Charge transfer resistance for Li-O_2 battery	158 Ω	93.6 Ω
Discharge platform for Li-O_2 battery (cycle 1)	2.81 V	2.85 V
Discharge platform for Li-O_2 battery (cycle 20)	2.78 V	2.81 V
Charge platform for Li-O_2 battery (cycle 1)	3.65 V	3.59 V
Charge platform for Li-O_2 battery (cycle 20)	4.10 V	3.67 V

References

S1 S. Trasatti, O. A. Petrii, *Pure Appl. Chem*. 1991, **63**, 711-734.

S2 C. C. L. McCrory, S. Jung, J. C. Peters and T. F. Jaramillo, *J Am Chem Soc*, 2013, **135**, 16977-16987.

S3 K. Zeng, H. Yu, Z. Sun, J. Yan, X. Zheng, Y. Jiang, W. Hu, J. Tian and R. Yang, *ACS Appl. Mater. Interfaces*, 2020, **12**, 39205-39214.

S4 P. Connor, J. Schuch, B. Kaiser and W. Jaegermann, *Z. Phys. Chem*, 2020; **234**, 979-994.

S5 P. Chen, T. Zhou, L. Xing, K. Xu, Y. Tong, H. Xie, L. Zhang, W. Yan, W. Chu, C. Wu and Y. Xie, *Angew Chem Int Edit*, 2017, **129**, 625-629.

S6 L. Gao, X. Li, Z. Yao, H. Bai, Y. Lu, C. Ma, S. Lu, Z. Peng, J. Yang, A. Pan and H. Huang, *J. Am. Chem. Soc*, 2019, **141**, 18083-18090.

S7 W. Zhong, Z. Lin, S. Feng, D. Wang, S. Shen, Q. Zhang, L. Gu, Z. Wang and B. Fang, *Nanoscale*, 2019, **11**, 4407-4413.

S8 M. Gao, W. Sheng, Z. Zhuang, Q. Fang, S. Gu, J. Jiang and Y. Yan, *J Am Chem Soc*, 2014, **136**, 7077-7084.

S9 S. Jiao, Z. Yao, M. Li, C. Mu, H. Liang, Y. Zeng and H. Huang, *Nanoscale*, 2019, **11**, 18894-18899.

S10 Y. Meng, W. Song, H. Huang, Z. Ren, S. Chen and S. L. Suib, *J Am Chem Soc*, 2014, **136**, 11452-11464.

S11 Q. Xue, Z. Pei, Y. Huang, M. Zhu, Z. Tang, H. Li, Y. Huang, N Li, H. Zhang and C. Zhi, *J Mater Chem A*, 2017, **5**, 20818-20823.

S12 J. Liu, L. Jiang, T. Zhang, J. Jin, L. Yuan and G. Sun, *Electrochim Acta*, 2016, **205**, 38-44.
S13 S. Hirai, S. Yagi, A. Seno, M. Fujioka, T. Ohno and T. Matsuda, *Rsc Adv*, 2016, **6**, 2019-2023.
S14 F. Bai, L. C. Xu, D. D. Wang, L. An, Z. Z. Hao and F. Li, Rsc Advances, 2021, 11, 1524-1530.